The block "PWM generator" generates the gate signals for the converter. Generally, a carrier generator, comparator circuit and a logic circuit to generate the "dead time" compose the "PWM generator". Figure 38 shows the screenshot of the schematic block diagram of the PWM modulator implemented in Quartus II environment for SPD modulation technique.

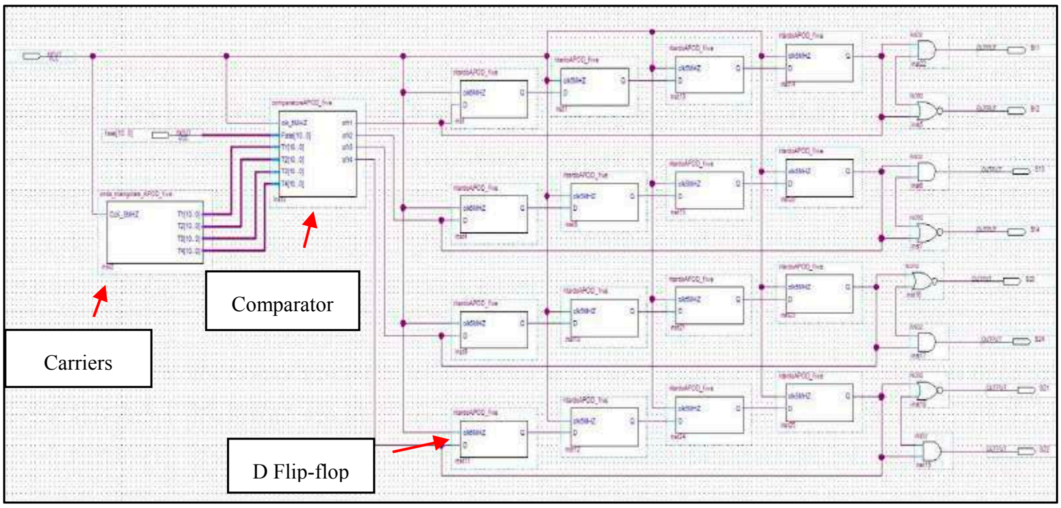

Figure 38. Screenshot of the schematic block diagram of the pulse width modulation (PWM) modulator implemented in Quartus II environment for SPD modulation technique.

Carrier waveform is generated by means a 13 bit up-down counter with a resolution of 1000 sample. The frequency of the clock reference is 10 MHz in order to obtain a frequency-switching equal to 10 kHz. The comparator circuit carried out the comparison between the modulating signal and carrier generator with a frequency equal to 10 MHz. The generation of the command signals of the components of the H-Bridge legs, as well as the obtainment of the dead-time for the protection of the series-connected components, is achieved through means of the logic circuit shown in Figure 39.

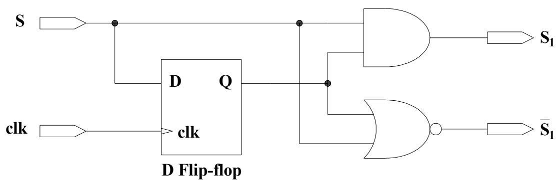

Figure 39. Logic circuit to generate the gate signals with dead time.

The delayed signal is obtained by using several cascaded-connected D flip-flops, whose number is dependent on the adopted clock signal. In order to obtain 400 ns of delay, four D flip-flops have been connected and managed with the 10 MHz clock signal. Figure 40 shows the simulation of the "PWM Generator" carried out in ModelSim environment relatively a phase of the converter.

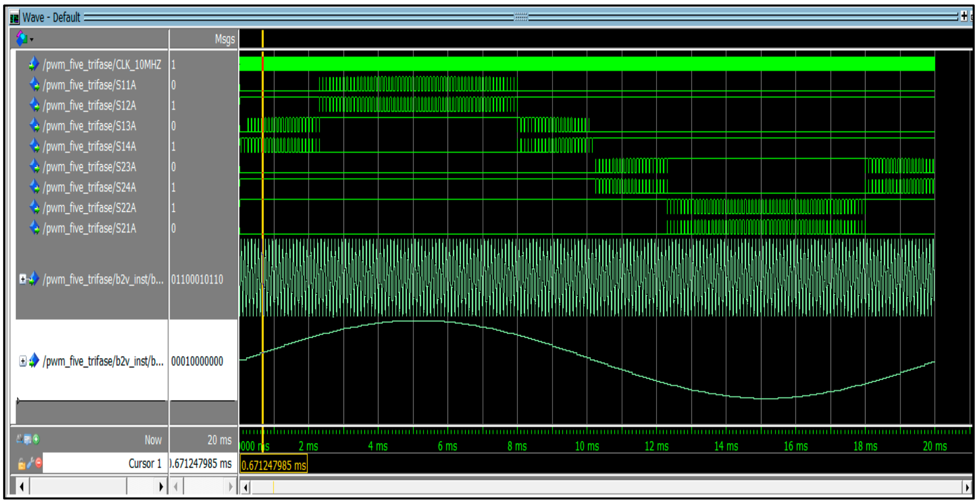

Figure 40. Simulation of the "PWM generator" in ModelSim environment.

From the technical features of the IRFB4115PBF reported in Table 12, the minimum dead time is equal to 100 ns, approximately. Thus, has been chosen for safe reason a dead time equal to 400 ns.

Figure 41 shows a screenshot of the experimental validation between gate signals of the same leg in order to establish the proper operation of the digital system.

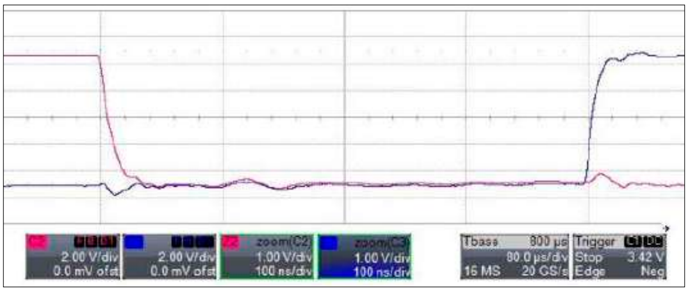

Figure 41. Experimental validation between gate signals of the same leg.

It should be noted that the dead time obtained is equal to 400 ns.

3.3. Model Validation

By the employment of the previously described test bench, the suggested techniques were experimentally implemented in order to validate the model of the system and to compare the simulation and experimental results.

The *Teledyne LeCroy WaveRunner 6Zi* acquisition system recorded the voltage waveforms. For the modulation PD, POD and APOD based techniques a sampling frequency of 50 MHz and a number of samples equal to 1 Ms were used; an observation window was choosen with a time interval equal to 20 ms.

The PS modulation techniques required an acquisition of 5 Ms of samples, equivalent to a sampling frequency of 250 MHz. The used tool to compare the simulation results and experimental results is the THD%, as reported in (27) [63]:

$$\mathrm{THD\%} = \sqrt{\frac{V_{rms}^2 - V_{rms,1}^2}{V_{rms,1}^2}} \cdot 100 \tag{27}$$

where V_{rms} is the root mean square (rms) value of the phase voltage and $V_{rms,1}$ defines the rms value of the fundamental harmonic.

Figures 42–44 show the comparison between the simulated (blue bars) and the experimental (yellow bars) THD% values obtained with Sinusoidal (Figure 42), THI (Figure 43) and SFO (Figure 44) as reference signals for each modulation techniques taken into account with the designed filter discussed in Section 2.2.

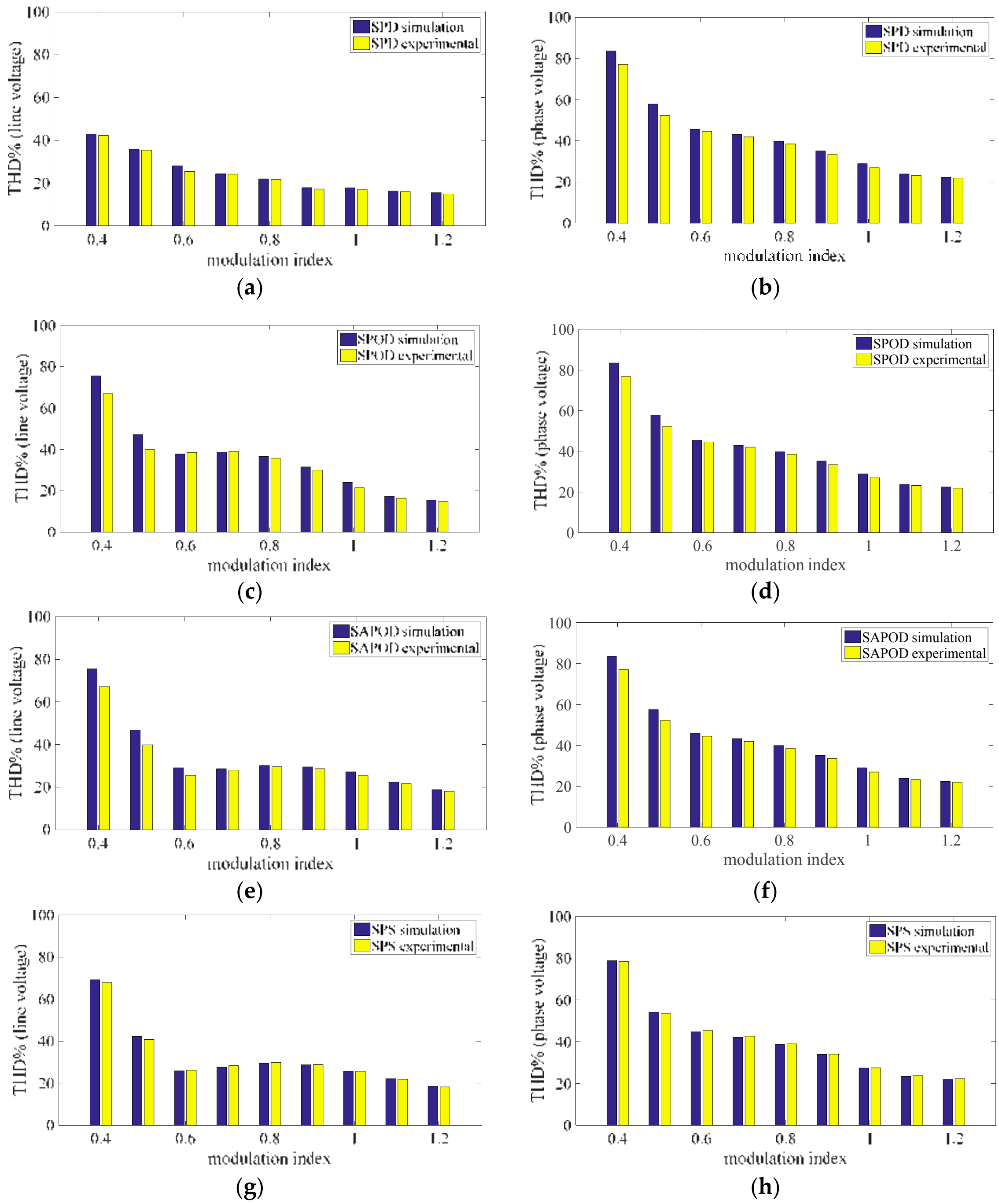

Figure 42. Comparison between the simulated (blue) and the experimental (yellow) THD% values: (**a**) SPD line voltage, (**b**) SPD phase voltage, (**c**) SPOD line voltage, (**d**) SPOD phase voltage, (**e**) SAPOD line voltage, (**f**) SAPOD phase voltage, (**g**) SPS line voltage, and (**h**) SPS phase voltage.

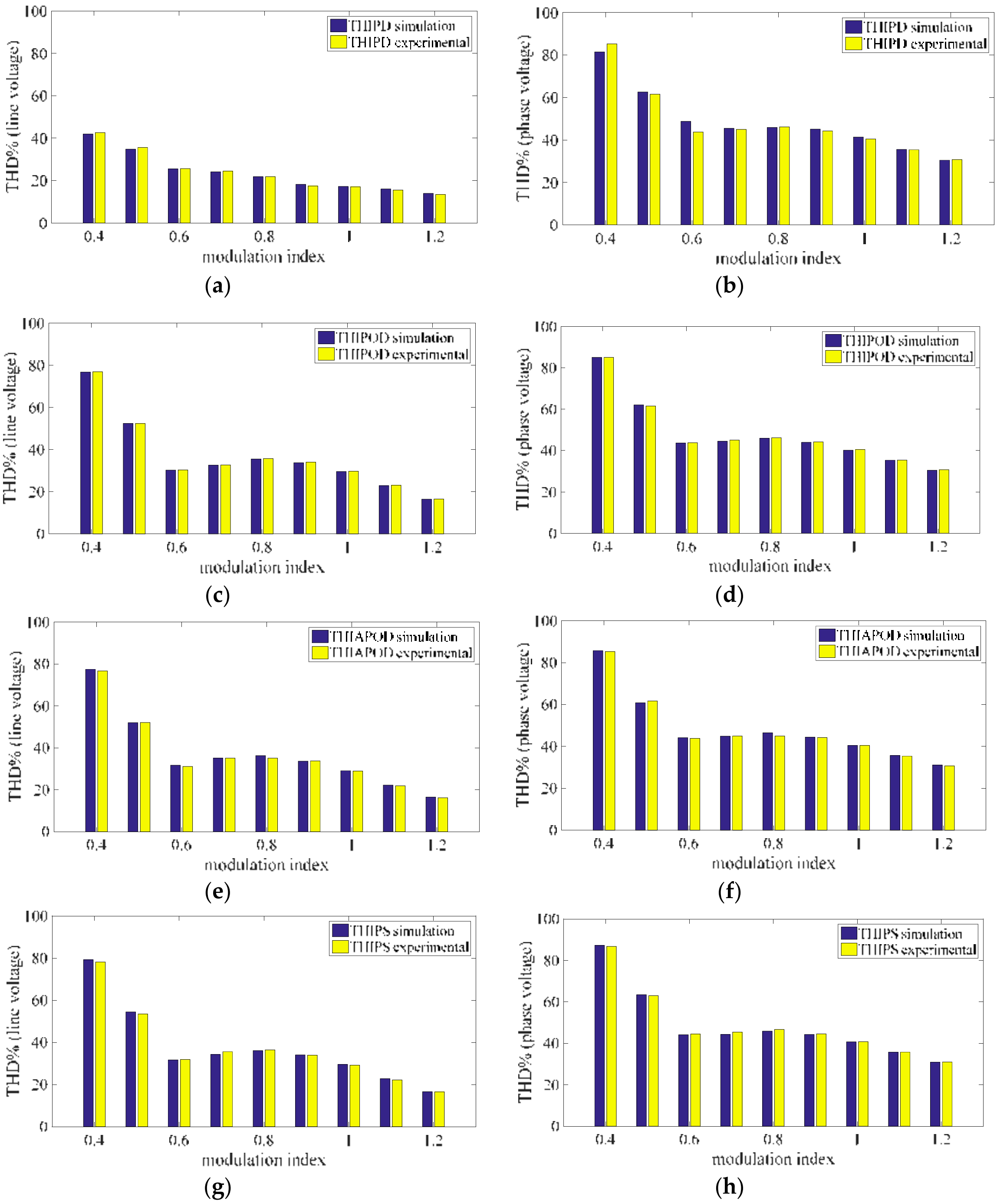

Figure 43. Comparison between the simulated (blue) and the experimental (yellow) THD% values: (**a**) THIPD line voltage, (**b**) THIPD phase voltage, (**c**) THIPOD line voltage, (**d**) THIPOD phase voltage, (**e**) THIAPOD line voltage, (**f**) THIAPOD phase voltage, (**g**) THIPS line voltage, and (**h**) THIPS phase voltage.

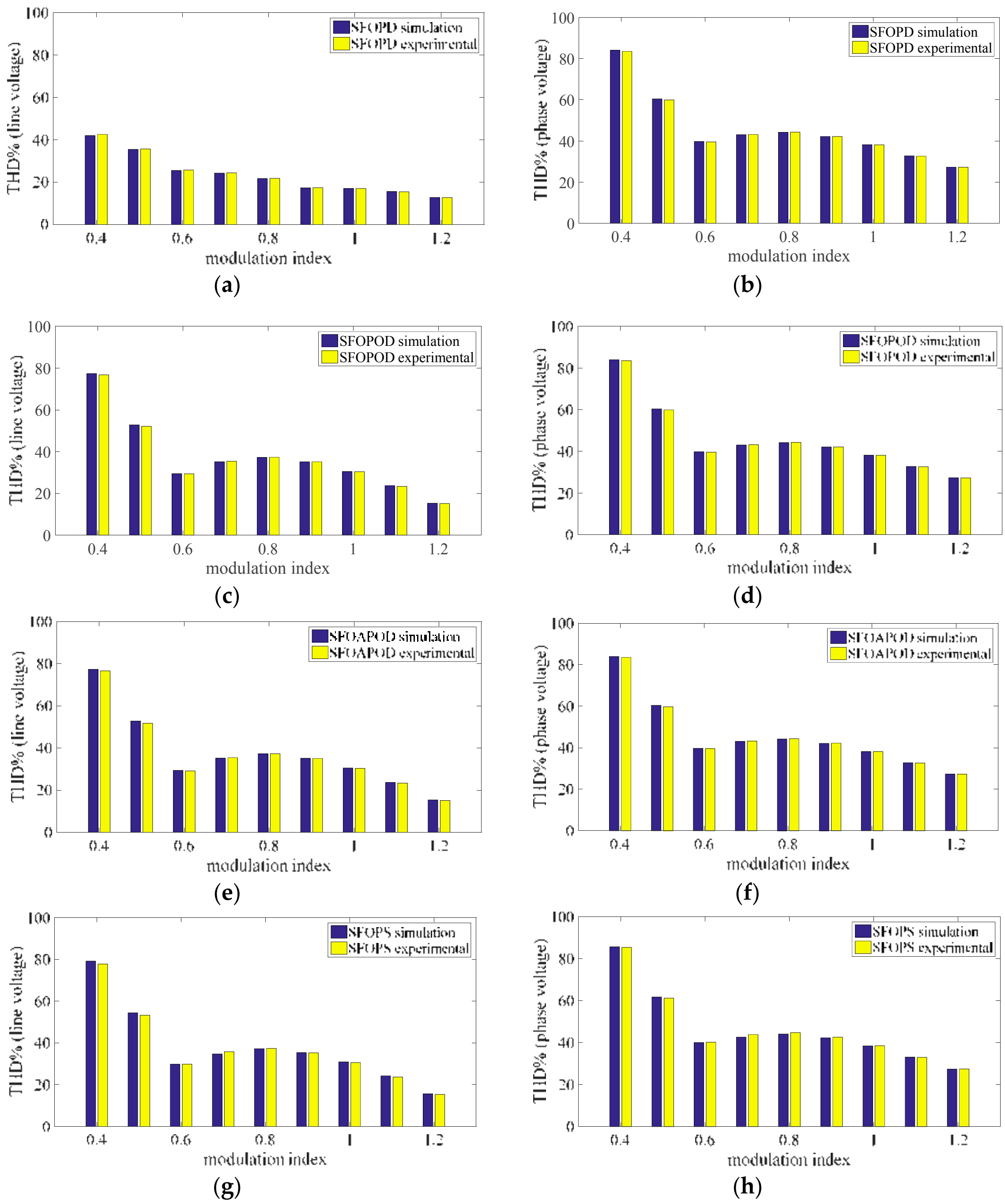

Figure 44. Comparison between the simulated (blue) and the experimental (yellow) THD% values: (**a**) SFOPD line voltage, (**b**) SFOPD phase voltage, (**c**) SFOPOD line voltage, (**d**) SFOPOD phase voltage, (**e**) SFOAPOD line voltage, (**f**) SFOAPOD phase voltage, (**g**) SFOPS line voltage, and (**h**) SFOPS phase voltage.

It should be noted that the simulated and experimental THD% presents similar values. For this reason, it is possible to establish the effectiveness of the model implemented.

Interesting comparison among the experimental THD% values for each reference signals taken into account, is shown in Figure 45. Modulation technique with PD as carrier signals and sinusoidal reference SPD seems to be the best solution in terms of the harmonic content. Moreover, also the SPS is a good solution for grid-connected applications.

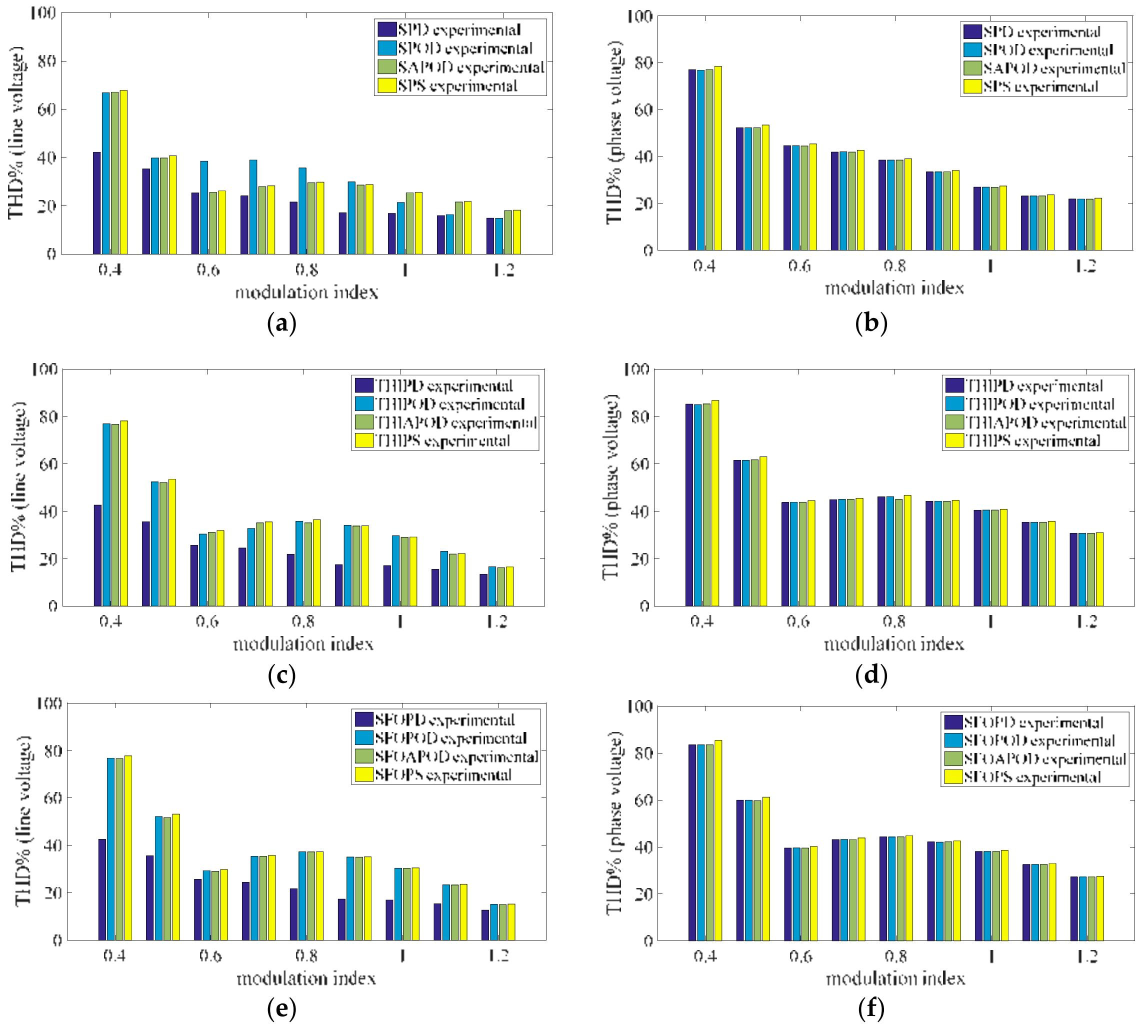

Figure 45. Comparison between the experimental THD% results: (**a**) Sinusoidal line voltage, (**b**) Sinusoidal phase voltage, (**c**) THI line voltage, (**d**) THI phase voltage, (**e**) SFO line voltage, and (**f**) SFO phase voltage.

In conclusion, modulation technique with PD as carrier signals and sinusoidal reference SPD present interesting results. Moreover, also the PS carrier signal is a good solution due to high order harmonic components respect other carrier signals.

In the next section, experimental validation of the grid-connected application is reported. The experimental validation considers only the SPD and SPS modulation techniques.

3.4. Grid Connected Application

Aim of this subsection is to validate the simulation results, reported in section "2.1 Performances evaluation", in which the best performances were obtained with SPD and SPS modulation techniques. In particular, the purpose is to validate by means experimental tests the effectiveness of the control strategy and the LCL filter. Thus, the experimental tests were carried out only with SPD and SPS modulation techniques.

3.4.1. Phase Disposition

Figure 46 shows the measured grid phase voltages and grid currents of the phase *a* and *b* obtained with SPD modulation technique at the rated power. It is interesting to note that the phase angle between voltage and current of the same phase is equal to zero. This result demonstrates the effectiveness of the control strategy because, as explained in the section "2.3 Controller Design", through the *d* component it is possible to control the active power while through the q component it is possible to control the reactive power. Thus, fixing q component of the current equal to zero and d component of the current equal to rated value (6A) it is possible to inject only active power on the grid as shown in Figure 46.

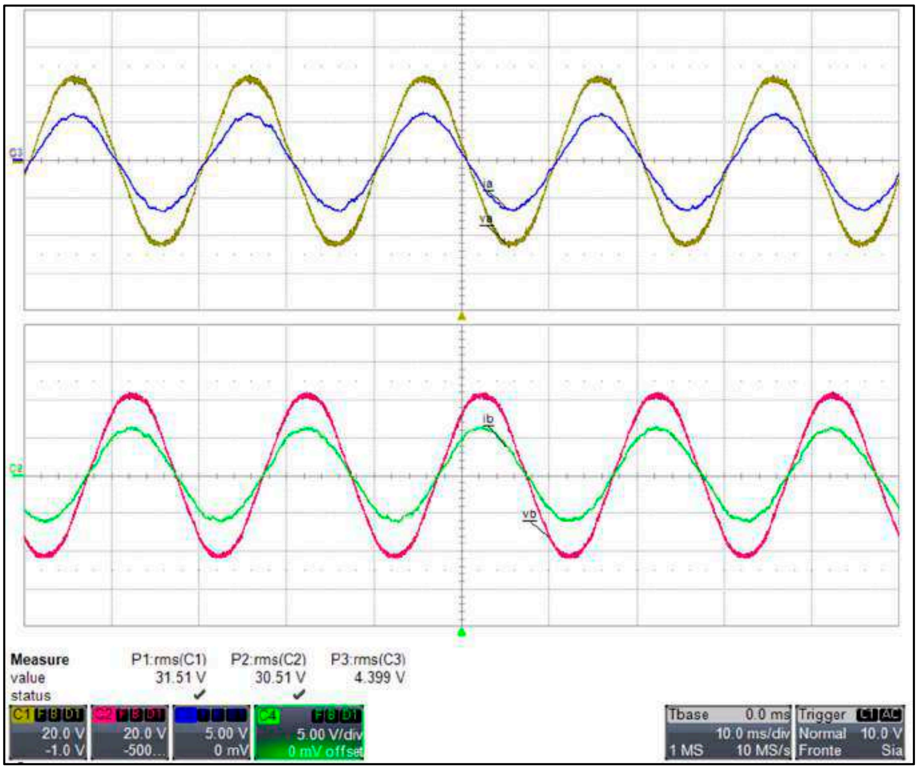

Figure 46. Measured grid voltages (20 V/div) and grid currents (5 A/div) of the phase a and b obtained with SPD at the rated power.

Figure 47 shows measured converter side current obtained with SPD at rated power while Figure 48 shows the measured grid side current in the same conditions.

First all, the differences in terms of the harmonic content between the trend of the converter side and grid side currents are evident. Moreover, a not perfect half-wave symmetry in the currents trend was observed. This phenomenon determined the present of the even-harmonics in the current.

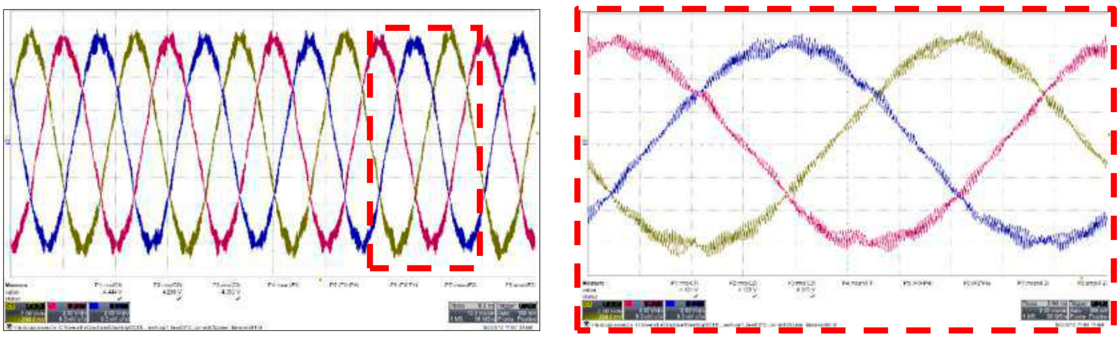

(**a**) (**b**)

Figure 47. Measured converter side currents (2 A/div) obtained with SPD at the rated power. (**a**) Ripple in different cycles; (**b**) Magnification of ripple.

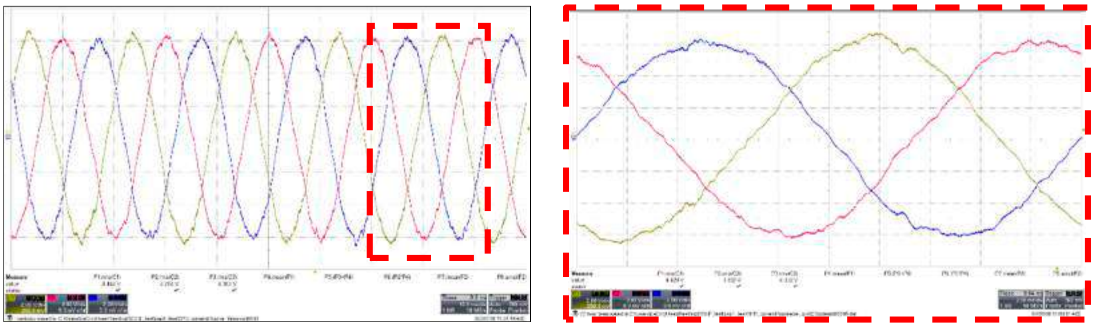

(**a**) (**b**)

Figure 48. Measured grid side currents (2 A/div) obtained with SPD at the rated power. (**a**) Ripple in different cycles; (**b**) Magnification of ripple.

Figure 49a shows the low order harmonics spectra of the grid side current at rated power. In the first all, it interesting to note that the amplitude of the lower order harmonics are below of the standard harmonic current limits defined by IEEE 1574 and IEC 61727 at the PCC. Nevertheless, as stated above are present the even-harmonics on the harmonic spectra. Interesting comparison between the harmonic spectra centered on switching frequency of the converter side current I_a (blue bars) and grid side current I_{ga} (yellow bars) is shown in Figure 49b. The lower values of the harmonics of the grid side current demonstrate the effectiveness of the LCL filter.

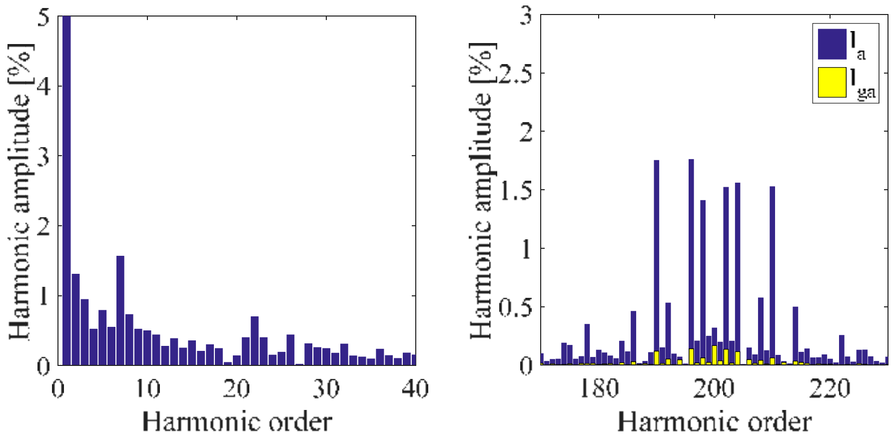

(**a**) (**b**)

Figure 49. Calculated (**a**) low order harmonics of the grid side current and (**b**) switching frequency harmonics spectra of the converter side and grid side currents.

In Table 14 are summarized the calculated THD% for different values of the grid side current injected. It should be noted that the THD% values increase when the current injected in the grid is reduced and it is less then 5% up to $I_n/2$.

Table 14. Experimental THD% of the converter and grid side currents, obtained with SPD, for different values of the injected current into the grid.

	$I_n/3$	$I_n/2$	$2I_n/3$	I_n
Converter side current	12.17%	7.82%	6.46%	5.88%
Grid side current	7.97%	4.78%	4.26%	3.72%

Figure 50 shows the measured line voltage of the converter at rated power. It interesting to note that the line voltage presents nine-level.

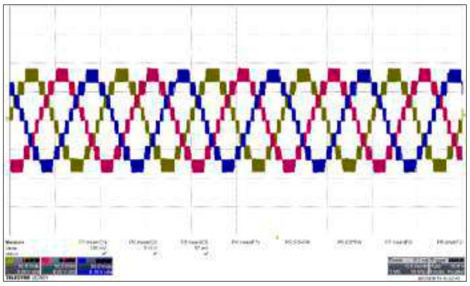

Figure 50. Measured line voltage of the converter at rated power.

Figure 51 shows the measured capacitor voltage of the LCL filter at rated power. The evident low harmonic content in the trend of the capacitor voltage demonstrate the efficacy of the LCL filter.

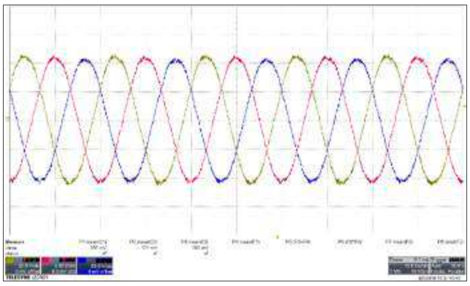

Figure 51. Measured capacitor voltage of the LCL filter at rated power.

As stated earlier, the second experimental tests have been carried out with SPS modulation techniques with the same filter used for SPD modulation techniques thank to the similar values obtained in the subsection "LCL filter Designs".

3.4.2. Phase Shifted

Figure 52 shows the measured grid phase voltages and grid currents obtained with SPS modulation technique at the rated power for each phase of the system.

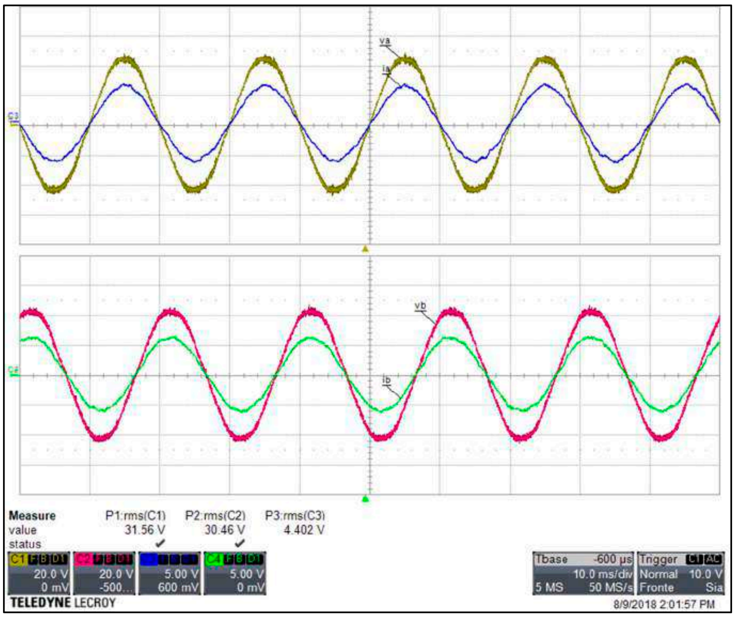

Figure 52. Measured grid voltages (20 V/div) and grid currents (5 A/div) of the phase a and b obtained with SPS at the rated power.

Also for this case, the phase angle between voltage and current of the same phase is equal to zero, thus this result demonstrates the efficacy of the control strategy.

Figures 53 and 54 show the measured converter side and grid side currents, respectively. As mentioned above, the currents trends present a not perfect half-wave symmetry and this phenomenon determined the even harmonics.

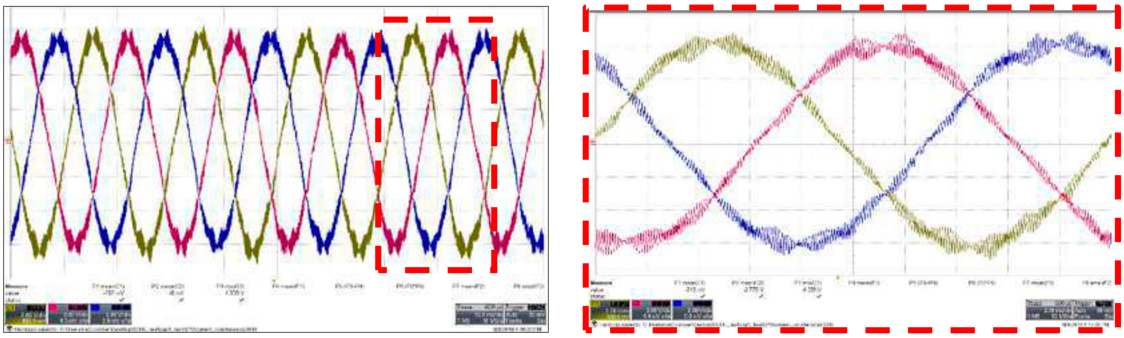

(**a**) (**b**)

Figure 53. Measured converter side currents (2 A/div) obtained with SPS at the rated power. (**a**) Ripple in different cycles; (**b**) Magnification of ripple.

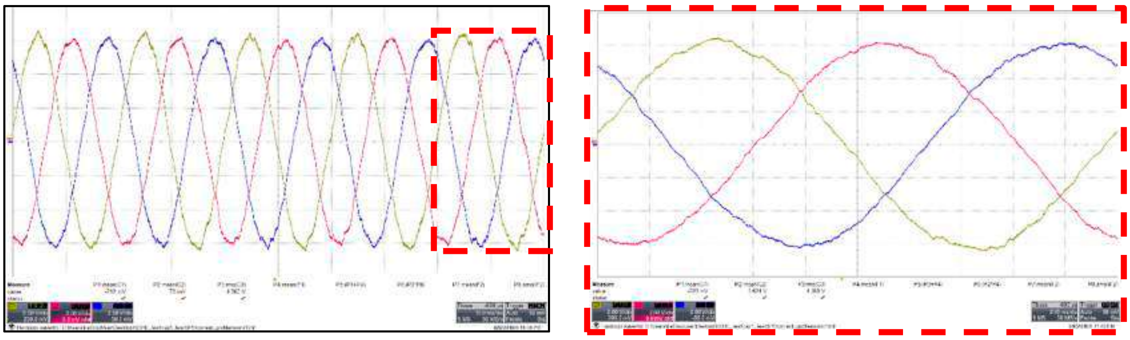

(**a**) (**b**)

Figure 54. Measured grid side currents (2 A/div) obtained with SPS at the rated power. (**a**) Ripple in different cycles; (**b**) Magnification of ripple.

Figure 55a shows the low order harmonics of the grid current at rated power. The amplitude of the all low order harmonics are less of the current limits reported in Table 1. However, by comparing the low order harmonic spectra of SPD and SPS, it can be noted that the second order harmonic is higher in SPS modulation technique. The presence of the even harmonics also is due to absence of the DC voltage control. Moreover, in both low order harmonic spectra of the SPD and SPS is predominant a seventh harmonic with similar value.

In Figure 55b is shown the comparison between the harmonic spectra centered on switching frequency of the converter side current I_a (blue bars) and grid side current I_{ga} (yellow bars). The lower values of the harmonics of the grid side current demonstrate the effectiveness of the LCL filter.

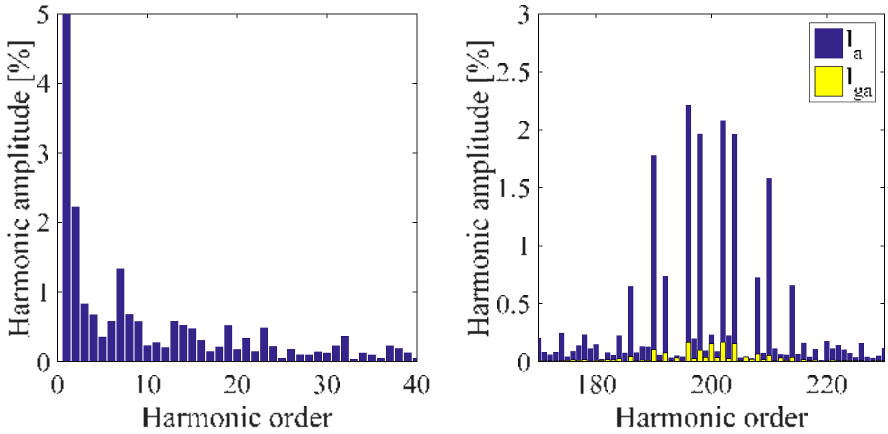

(**a**) (**b**)

Figure 55. Calculated (**a**) low order harmonics of the grid side current and (**b**) switching frequency harmonics spectra of the converter side and grid side currents.

In Table 15 are summarized the calculated THD% for different values of side current injected in the grid. The THD% values obtained with SPS are similar respect to the previously calculated with SPD. This is an interesting result, because the modulation techniques PS based are more versatile respect to the others multicarrier modulation techniques for grid connected applications like PV systems, for example. The modulation techniques PS based allow to control each H-Bridge like a single-phase inverter and it is possible to use innovative control algorithms especially designed in dependence of the application.

Table 15. Experimental THD% of the converter and grid side currents, obtained with SPS, for different values of the injected current into the grid.

	$I_n/3$	$I_n/2$	$2I_n/3$	I_n
Converter side current	12.28%	8.41%	6.80%	5.64%
Grid side current	7.42%	4.45%	3.91%	3.33%

In addition, the line voltage build with the SPS modulation technique has nine level, as shown in Figure 56.

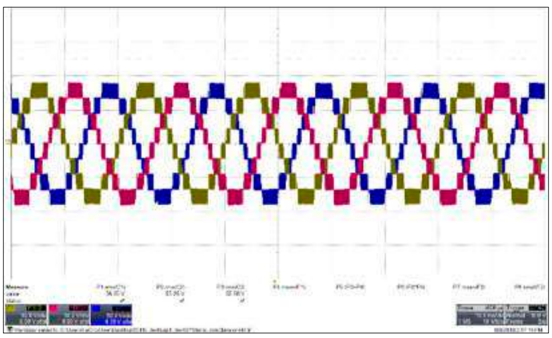

Figure 56. Measured line voltage of the converter at rated power.

Figure 57 shows the measured capacitor voltage of the LCL filter with an evident low harmonic content that also in this case demonstrate the efficacy of the LCL filter.

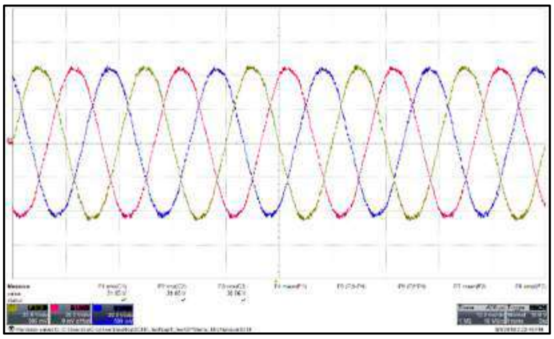

Figure 57. Measured capacitor voltage of the LCL filter at rated power.

4. Discussion

In order to face the harmonic distortion problem, two issue can be distinctly taken into account: the generation of harmonics and their suppression. Although the approach is not purely dichotomous, since a lower generation corresponds to an easier suppression, here the main results of this work can be approached with an etiological methodology.

The modulation techniques with PD as carrier signals shows a harmonic spectrum of the phase voltage with a predominant harmonic centered on the switching frequency and side band harmonics (Figure 10). By considering the modulation with POD and APOD as carriers, in the spectra, the harmonic component at switching frequency does not appear but there are only side bands (Figure 16). By considering the modulation with PS disposition, the harmonics are centered around four times the switching frequency, are present only side bands harmonics like in modulation techniques POD and APOD based (Figure 25).

In order to reduce the harmonics in the grid side, a filtering system is correctly designed. For the PD based modulation techniques, the converter side inductance L and grid side inductance L_g present the lower values (Table 4). Higher value of the converter side inductance were obtained with THIPOD modulation technique, phenomenon attributable to the higher number of the side band harmonics generated by POD carrier signals. Figure 14 (PD), 23 (POD and APOD) and 29 (PS) show the performances of the filtering by considering the different modulation techniques. For each techniques, the third harmonic of injected current is much reduced, so the comparison moves on the fifth harmonic: PD is around 1%, POD and APOD less than 0.5%, PS around 2%. Excellent performance of THIPOD for its very low values of fifth and also seventh harmonic, are remarkable, but the side inductance L is eight times the value for PD ones. By analyzing Figure 29, low order harmonics contents are present, in particular besides the fifth, seventh is predominant. Modulation techniques PS based have the higher values of the lower order harmonics compared with all modulation techniques previously described.

In conclusion, modulation techniques PD based allow obtaining good results in terms of the harmonic content on the grid current with the lower values of the LCL filter parameters. In particular, SPD represent the best solution.

The previous described good results are validated in Figure 45 with the experimental test phase; moreover, it is possible to find an experimental behavior better than the simulated one for SPD for different modulation indexes.

Finally, the approach was validated for a grid-connected system by exploiting the three-phase Variac to grid interface. Different current values were injected in the power grid, Tables 14 and 15 report that the THD% remained below the 4%, 3.72% for SPD and 3.33% for SPS techniques.

By considering the work of Colak et al. [64], as the number of levels in multilevel inverter increases, the THD in the output voltage reduces, but the drawback of increasing the levels is that that the control circuit becomes hard challenges. A comparison can be done with recent results found in literature. Kavali and Mittal obtained by MATLAB based simulation with SIMULINK environment interesting results for their single-phase five level CHBMI topology with sinusoidal pulse width modulation schemes [37]. For PD the THD was reduced to 5.69%; in case of POD it was 5.75%; for APOD it was

5.73%; the THD was 7.42% in case of PS. Results obtained in the present work follow those obtained in [37], the obtained THDs are below, and add an experimental validation to them.

5. Conclusions

As previously described, the PWM modulation techniques found large use in many industrial applications thanks their main features as easy implementation in electronic control systems, low computational cost and high flexibility. Moreover, for grid-connected applications the PWM modulation techniques are the best solution due to the lower amplitude of the low-order harmonics, reducing the filter requirements. Thus, in this work a detailed analysis taking into account all PWM modulation techniques, the LCL filter requirements and the real time implementation issues in FPGA-based prototype control board for a grid-connected three-phase five-level CHBMI, was presented.

Firstly, through a simple step-by-step procedure to design LCL filter for each modulation techniques taken into account, it was demonstrated that the lower values of the filter parameters are obtained for modulation techniques employing sinusoidal as reference signals. These interesting results were confirmed by the experimental validation of the THD% values. In particular, the SPD and SPS showed the best results in terms of the THD% values. Then, the experimental tests was focused by using the SPD and SPS modulation techniques in order to inject in the power grid different values of current through the specially designed LCL filter. Notably, the experimental tests confirmed the effectiveness of the LCL filter. The amplitude of the lower order harmonics are below of the standard harmonic current limits at the point of common coupling. Nevertheless, appeared even-harmonics on the amplitude spectra. Finally, it is possible to claim that the modulation technique SPS is the best solution for all grid-connected applications where it is necessary to control the power flow of the DC sources separately.

Funding: This research received no external funding.

Acknowledgments: This work was financially supported by MIUR-Ministero dell'Istruzione dell'Università e della Ricerca (Italian Ministry of Education, University and Research), by SDESLab (Sustainable Development and Energy Saving Laboratory), and LEAP (Laboratory of Electrical Applications) of the University of Palermo.

Conflicts of Interest: The author declares no conflict of interest.

References

1. Rashid, M.H. *Power Electronics Handbook, Devices, Circuits and Applications*, 3rd ed.; Butherworth-Heirmann is an imprint of Elsevier; Pearson Education Limited: New York, NY, USA, 2011.
2. Rodriguez, J.; Lai, J.-S.; Peng, F.Z. Multilevel inverters: A survey of topologies, controls, and applications. *IEEE Trans. Ind. Electron.* **2002**, *49*, 724–738. [CrossRef]
3. Malinowski, M.; Gopakumar, K.; Rodriguez, J.; Perez, M.A. A Survey on Cascaded Multilevel Inverters. *IEEE Trans. Ind. Electron.* **2010**, *57*, 2197–2206. [CrossRef]
4. Kouro, S.; Malinowski, M.; Gopakumar, K.; Pou, J.; Franquelo, L.G.; Wu, B.; Rodriguez, J.; Perez, M.A.; Leon, J.I. Recent Advances and Industrial Applications of Multilevel Converters. *IEEE Trans. Ind. Electron.* **2010**, *57*, 2553–2580. [CrossRef]
5. El-Hosainy, A.; Hamed, H.A.; Azazi, H.Z.; El-Kholy, E.E. A review of multilevel inverter topologies, control techniques and applications. In Proceedings of the 2017 Nineteenth International Middle East Power Systems Conference (MEPCON), Cairo, Egypt, 19–21 December 2017; pp. 1265–1275.
6. McGrath, B.P.; Holmes, D.G. Multicarrier PWM strategies for multilevel inverters. *IEEE Trans. Ind. Electron.* **2002**, *49*, 858–867. [CrossRef]
7. McGrath, B.P.; Holmes, D.G. A comparison of multicarrier PWM strategies for cascaded and neutral point clamped multilevel inverters. In Proceedings of the 2000 IEEE 31st Annual Power Electronics Specialists Conference, Conference Proceedings (Cat. No.00CH37018), Galway, Ireland, 23–23 June 2000; Volume 2, pp. 674–679.

8. Jeevananthan, S.; Madhavan, R.; Padmanabhan, T.S.; Dananjayan, P. State-of-the-art of Multi-Carrier Modulation Techniques for Seven Level Inverter: A Critical Evaluation and Novel Submissions based on Control Degree of Freedom. In Proceedings of the 2006 IEEE International Conference on Industrial Technology, Mumbai, India, 15–17 December 2006; pp. 1269–1274.
9. Holmes, D.G.; Lipo, T.A. *Pulse Width Modulation for Power Converters*; IEEE Press series on Power Engineering; Wiley Interscience: New York, NY, USA, 2004.
10. Schettino, G.; Benanti, S.; Buccella, C.; Caruso, M.; Castiglia, V.; Cecati, C.; Di Tommaso, A.O.; Miceli, R.; Romano, P.; Viola, F. Simulation and experimental validation of multicarrier PWM techniques for three-phase five-level cascaded H-bridge with FPGA controller. *Int. J. Renew. Energy Res.* **2017**, *7*, 1383–1394.
11. Schettino, G.; Buccella, C.; Caruso, M.; Cecati, C.; Castiglia, V.; Miceli, R.; Viola, F. Overview and experimental analysis of MC SPWM techniques for single-phase five level cascaded H-bridge FPGA controller-based. In Proceedings of the IECON 2016—42nd Annual Conference of the IEEE Industrial Electronics Society, Florence, Italy, 23–26 October 2016; pp. 4529–4534.
12. Benanti, S.; Buccella, C.; Caruso, M.; Castiglia, V.; Cecati, C.; Di Tommaso, A.O.; Miceli, R.; Romano, P.; Schettino, G.; Viola, F. Experimental analysis with FPGA controller-based of MC PWM techniques for three-phase five level cascaded H-bridge for PV applications. In Proceedings of the 2016 IEEE International Conference on Renewable Energy Research and Applications (ICRERA), Birmingham, UK, 20–23 November 2016; pp. 1173–1178.
13. Castiglia, V.; Livreri, P.; Miceli, R.; Raciti, A.; Schettino, G.; Viola, F. Performances of a three-phase five-level cascaded H-bridge inverter with phase shifted B-spline based modulation techniques. In Proceedings of the 6th International Conference on Renewable Energy Research and Applications (ICRERA), San Diego, CA, USA, 5–8 November 2017; pp. 1192–1197.
14. Schettino, G.; Castiglia, V.; Genduso, F.; Livreri, P.; Miceli, R.; Romano, P.; Viola, F. Simulation of a single-phase five-level cascaded H-Bridge inverter with multicarrier SPWM B-Spline based modulation techniques. In Proceedings of the 12th International Conference on Ecological Vehicles and Renewable Energies (EVER), Monte Carlo, Monaco, 11–13 April 2017.
15. Grahame, D.; Buccella, C.; Cecati, C.; Latafat, H. Digital Control of Power Converters—A Survey. *IEEE Trans. Ind. Inf.* **2012**, *8*, 437–447. [CrossRef]
16. Monmasson, E.; Cirstea, M.N. FPGA Design Methodology for Industrial Control Systems—A Review. *IEEE Trans. Ind. Electron.* **2007**, *54*, 1824–1842. [CrossRef]
17. Monmasson, E.; Idkhajine, L.; Cirstea, M.N.; Bahri, I.; Tisan, A.; Naouar, M.W. FPGAs in Industrial Control Applications. *IEEE Trans. Ind. Inf.* **2011**, *7*, 224–243. [CrossRef]
18. Rodríguez-Andina, J.J.; Valdés-Peña, M.D.; Moure, M.J. Advanced Features and Industrial Applications of FPGAs—A Review. *IEEE Trans. Ind. Inf.* **2015**, *11*, 853–864. [CrossRef]
19. Naouar, M.W.; Monmasson, E.; Naassani, A.A.; Slama-Belkhodja, I.; Patin, N. FPGA-Based Current Controllers for AC Machine Drives—A Review. *IEEE Trans. Ind. Inf.* **2007**, *54*, 1907–1925. [CrossRef]
20. Kala, P.; Arora, S. A comprehensive study of classical and hybrid multilevel inverter topologies for renewable energy applications. *Renew. Sustain. Energy Rev.* **2017**, *76*, 905–931. [CrossRef]
21. Venkataramanaiah, J.; Suresh, Y.; Panda, A.K. A review on symmetric, asymmetric, hybrid and single DC sources based multilevel inverter topologies. *Renew. Sustain. Energy Rev.* **2017**, *76*, 788–812. [CrossRef]
22. Jana, J.; Saha, H.; Bhattacharya, K.D. A review of inverter topologies for single-phase grid-connected photovoltaic systems. *Renew. Sustain. Energy Rev.* **2017**, *72*, 1256–1270. [CrossRef]
23. Monica, P.; Kowsalya, M. Control strategies of parallel operated inverters in renewable energy application: A review. *Renew. Sustain. Energy Rev.* **2016**, *65*, 885–901. [CrossRef]
24. Son, Y.; Kim, J. A Novel Phase Current Reconstruction Method for a Three-Level Neutral Point Clamped Inverter (NPCI) with a Neutral Shunt Resistor. *Energies* **2018**, *11*, 2616. [CrossRef]
25. Ye, Z.; Chen, A.; Mao, S.; Wang, T.; Yu, D.; Deng, X. A Novel Three-Level Voltage Source Converter for AC–DC–AC Conversion. *Energies* **2018**, *11*, 1147. [CrossRef]
26. Ricco, M.; Mathe, L.; Monmasson, E.; Teodorescu, R. FPGA-Based Implementation of MMC Control Based on Sorting Networks. *Energies* **2018**, *11*, 2394. [CrossRef]
27. Wu, Z.; Chu, J.; Gu, W.; Huang, Q.; Chen, L.; Yuan, X. Hybrid Modulated Model Predictive Control in a Modular Multilevel Converter for Multi-Terminal Direct Current Systems. *Energies* **2018**, *11*, 1861. [CrossRef]

28. Talon Louokdom, E.; Gavin, S.; Siemaszko, D.; Biya-Motto, F.; Essimbi Zobo, B.; Marchesoni, M.; Carpita, M. Small-Scale Modular Multilevel Converter for Multi-Terminal DC Networks Applications: System Control Validation. *Energies* **2018**, *11*, 1690. [CrossRef]
29. Kumar, N.; Saha, T.K.; Dey, J. Modeling, control and analysis of cascaded inverter based grid-connected photovoltaic system. *Int. J. Electr. Power Energy Syst.* **2016**, *78*, 165–173. [CrossRef]
30. Ravi, A.; Manoharan, P.S.; Anand, J.V. Modeling and simulation of three phase multilevel inverter for grid connected photovoltaic systems. *Sol. Energy* **2011**, *85*, 2811–2818. [CrossRef]
31. Rajkumar, M.V.; Manoharan, P.S. FPGA based multilevel cascaded inverters with SVPWM algorithm for photovoltaic system. *Sol. Energy* **2013**, *87*, 229–245. [CrossRef]
32. Prabaharan, N.; Palanisamy, K. Analysis and integration of multilevel inverter configuration with boost converters in a photovoltaic system. *Energy Convers. Manag.* **2016**, *128*, 327–342. [CrossRef]
33. Iero, D.; Carbone, R.; Carotenuto, R.; Felini, C.; Merenda, M.; Pangallo, G.; Della Corte, F.G. SPICE modelling of a complete photovoltaic system including modules, Energy storage elements and a multilevel inverter. *Sol. Energy* **2014**, *107*, 338–350. [CrossRef]
34. Javad, O.; Shayan, E.; Ali, M. Compensation of voltage sag caused by partial shading in grid-connected PV system through the three-level SVM inverter. *Sustain. Energy Technol. Assess.* **2016**, *18*, 107–118.
35. Prabaharan, N.; Palanisamy, K. A Single Phase Grid Connected Hybrid Multilevel Inverter for Interfacing Photo-voltaic System. *Energy Procedia* **2016**, *103*, 250–255. [CrossRef]
36. Rahim, N.A.; Ping, H.W.; Selvaraj, J. Elimination of harmonics in photovoltaic seven-level inverter with Newton-Raphson optimization. *Procedia Environ. Sci.* **2013**, *17*, 519–528.
37. Kavali, J.; Mittal, A. Analysis of various control schemes for minimal Total Harmonic Distortion in cascaded H-bridge multilevel inverter. *J. Electr. Syst. Inf. Technol.* **2016**, *3*, 428–441. [CrossRef]
38. Al-Othman, A.K.; Abdelhamid, T.H. Elimination of harmonics in multilevel inverters with non-equal dc sources using PSO. In Proceedings of the 2008 13th International Power Electronics and Motion Control Conference (EPE-PEMC 2008), Poznan, Poland, 1–3 September 2008; pp. 756–764.
39. Marzoughi, A.; Imaneini, H.; Moeini, A. An optimal selective harmonic mitigation technique for high power converters. *Int. J. Electr. Power Energy Syst.* **2013**, *49*, 34–39. [CrossRef]
40. Voltage Characteristics of Electricity Supplied by Public Electricity Networks. Available online: http://fs.gongkong.com/files/technicalData/201110/2011100922385600001.pdf (accessed on 15 January 2018).
41. Personen, M.A. Harmonics characteristic parameters methods of study estimates of existing values in the network. *Electra* **1981**, *77*, 35–54.
42. Electromagnetic Compatibility (EMC)–Part 3-7: LIMITS–Assessment of Emission Limits for the Connection of Fluctuating Installations to MV, HV and EHV Power Systems. Available online: https://ieeexplore.ieee.org/document/6232421/ (accessed on 15 January 2018).
43. Letha, S.S.; Thakur, T.; Kumar, J. Harmonic elimination of a photo-voltaic based cascaded H-bridge multilevel inverter using PSO (particle swarm optimization) for induction motor drive. *Energy* **2016**, *107*, 335–346. [CrossRef]
44. Rao, G.N.; Raju, P.S.; Sekhar, K.C. Harmonic elimination of cascaded H-bridge multilevel inverter based active power filter controlled by intelligent techniques. *Int. J. Electr. Power Energy Syst.* **2014**, *61*, 56–63.
45. Panda, A.K.; Patnaik, S.S. Analysis of cascaded multilevel inverters for active harmonic filtering in distribution networks. *Int. J. Electr. Power Energy Syst.* **2015**, *66*, 216–226. [CrossRef]
46. Mohan, N.; Undeland, T.M.; Robbins, W.P. *Power Electronics–Converter, Applications and Design*, 3rd ed.; John Wiley & Sons, Inc.: New York, NY, USA, 1989.
47. Miceli, R.; Schettino, G.; Viola, F. A Novel Computational Approach for Harmonic Mitigation in PV Systems with Single-Phase Five-Level CHBMI. *Energies* **2018**, *11*, 2100. [CrossRef]
48. IEEE. *IEEE Application Guide for IEEE Std 1547, IEEE Standard for Interconnecting Distributed Resources with Electric Power Systems IEEE Standard 1547.2-2008*; IEEE: Biloxi, MI, USA, 2009.
49. Crăciun, B.I.; Kerekes, T.; Séra, D.; Teodorescu, R. Overview of recent Grid Codes for PV power integration. In Proceedings of the 2012 13th International Conference on Optimization of Electrical and Electronic Equipment (OPTIM), Brasov, Romania, 24–26 May 2012; pp. 959–965.
50. Beres, R.N.; Wang, X.; Liserre, M.; Blaabjerg, F.; Bak, C.L. A Review of Passive Power Filters for Three-Phase Grid-Connected Voltage-Source Converters. *IEEE J. Emerg. Sel. Top. Power Electron.* **2016**, *4*, 54–69. [CrossRef]

51. Liserre, M.; Blaabjerg, F.; Dell'Aquila, A. Step-by-step design procedure for a grid-connected three-phase PWM Voltage Source Converter. *Int. J. Electron.* **2004**, *91*, 445–460. [CrossRef]
52. Liserre, M.; Blaabjerg, F.; Hansen, S. Design and control of an LCL-filter-based three-phase active rectifier. *IEEE Trans. Ind. Appl.* **2005**, *41*, 1281–1291. [CrossRef]
53. Bojrup, M. Advanced Control of Active Filters in a Battery Charger Application. Ph.D. Thesis, Lund University of Technology, Lund, Sweden, 1999.
54. Teodorescu, R.; Liserre, M.; Rodriguez, P. *Grid Converters for Photovoltaic and Wind Power System*; John Wiley & Sons, Ltd.: New York, NY, USA, 2011; ISBN 978-0-470-05751-3.
55. Blaabjerg, F.; Teodorescu, R.; Liserre, M.; Timbus, A.V. Overview of Control and Grid Synchronization for Distributed Power Generation Systems. *IEEE Trans. Ind. Electron.* **2006**, *53*, 1398–1409. [CrossRef]
56. Timbus, A.; Liserre, M.; Teodorescu, R.; Blaabjerg, F. Synchronization methods for three phase distributed power generation systems—An overview and evaluation. In Proceedings of the 2005 IEEE 36th Power Electronics Specialists Conference, Recife, Brazil, 16 June 2005; pp. 2474–2481.
57. International Rectifier, "Data Sheet IRFB4115PbF". Available online: www.irf.com (accessed on 15 January 2018).
58. ALTERA. *Cyclone III Device Handbook—Volume 1*; ALTERA: San Jose, CA, USA, December 2011; Available online: http://www.altera.com (accessed on 15 January 2018).
59. ALTERA. *Cyclone III Device Handbook—Volume 2*; ALTERA: San Jose, CA, USA, July 2012; Available online: http://www.altera.com (accessed on 15 January 2018).
60. ALTERA. *Quartus II Handbook Version 13.1—Volume 1: Design and Synthesis*; ALTERA: San Jose, CA, USA, November 2013; Available online: http://www.altera.com (accessed on 15 January 2018).
61. ALTERA. *Quartus II Handbook Version 13.1—Volume 2: Design Implementation and Optimization*; ALTERA: San Jose, CA, USA, November 2013; Available online: http://www.altera.com (accessed on 15 January 2018).
62. Zwoliński, M. *Digital System Design with VHDL*, 2nd ed.; Pearson-Prentice Hall: Upper Saddle River, NJ, USA, 2004.
63. Dordevic, O.; Jones, M.; Levi, E. Analytical Formulas for Phase Voltage RMS Squared and THD in PWM Multiphase Systems. *IEEE Trans. Power Electron.* **2015**, *30*, 1645–1656. [CrossRef]
64. Colak, I.; Kabalci, E.; Bayindir, R. Review of multilevel voltage source inverter topologies and control schemes. *Energy Convers. Manag.* **2011**, *52*, 1114–1128. [CrossRef]